A lunar cone in Mare Crisium by Raffaello Lena

The Crisium Basin formed near the end of the period of high cratering flux, dated as 4.05-4.13 billion years ago or Giga annum-Ga (Wilhelms, 1973). Mare Spumans and Mare Undarum are presumed to be within the continuous Crisium ejecta. The surrounding basin material is of the Nectarian epoch, with the mare basalt being of the Upper Imbrian epoch (Olson and Wilhelms, 1973 and references therein). After the formation of the Crisium Basin, mare materials were emplaced in the central basin and in the peripheral troughs around the basin. Most of the mare materials in the circum-basin troughs consist of localized, isolated patches which are bounded by structures approximately radial and concentric to the basin. Mare Undarum and the northern part of Mare Spumans occupy a trough between the 340- and 485-km raised rings (De Hon, 1975).

The Crisium Basin concentric structure consists of a series of raised rings and intervening troughs. Three rugged rings are delineated in the circum-mare terra and another lies within the mare (Wilhelms, 1973). Rings are approximately 210, 250, 340, and 485 km from the basin center. The raised rings are composed of pre-basin rock and overlying basin ejecta.

An overview of the geologic setting of Mare Crisium is reported by Lu et al. (2021). The earliest basaltic volcanism in the Crisium basin erupted around 3.74 Ga, forming the oldest middle-to-high-Ti mare basalts (6~10 wt % TiO_2); basalt filled most area of the Crisium basin during the Imbrian period, defined as Im1 unit. The subsequent low-to-middle basaltic volcanism occurred and flooded the center and western area (i.e., Im2 and Im3 unit) at ~3.5 Ga, superposed on the prominent high-Ti basalts (Lu et al., 2021). Furthermore Im2 is the largest maria plain. This geologic unit contains a medium TiO_2 content (4~5 wt %) and medium-to-high FeO content (15~22 wt %). The Eratosthenian-age basaltic volcanism erupted, and widespread lava flows filled the northern and eastern area of the Crisium basin. In this period, large craters Picard and Peirce were generated and the subsurface high-TiO_2 basalt in the western area was excavated. In the Copernican period, a wide range of volcanism has ceased, but the impact events continued to reshape the terrain and garden the surface materials of the Crisium basin. Contaminated ejecta and distal material transports from Proclus and other craters in the highlands could overlap and complicate the mixing of local mare basalts characterized by very low-Ti (~1 wt %) materials (Lu et al., 2021).

In this note I will describe a horseshoe feature, located in Mare Crisium, at 61.9°E and 18.5°N including telescopic images.

A terrestrial telescopic image of this examined feature is shown in Fig. 1. It was taken by Teodorescu on October 3, 2020 at 23:02 UT.

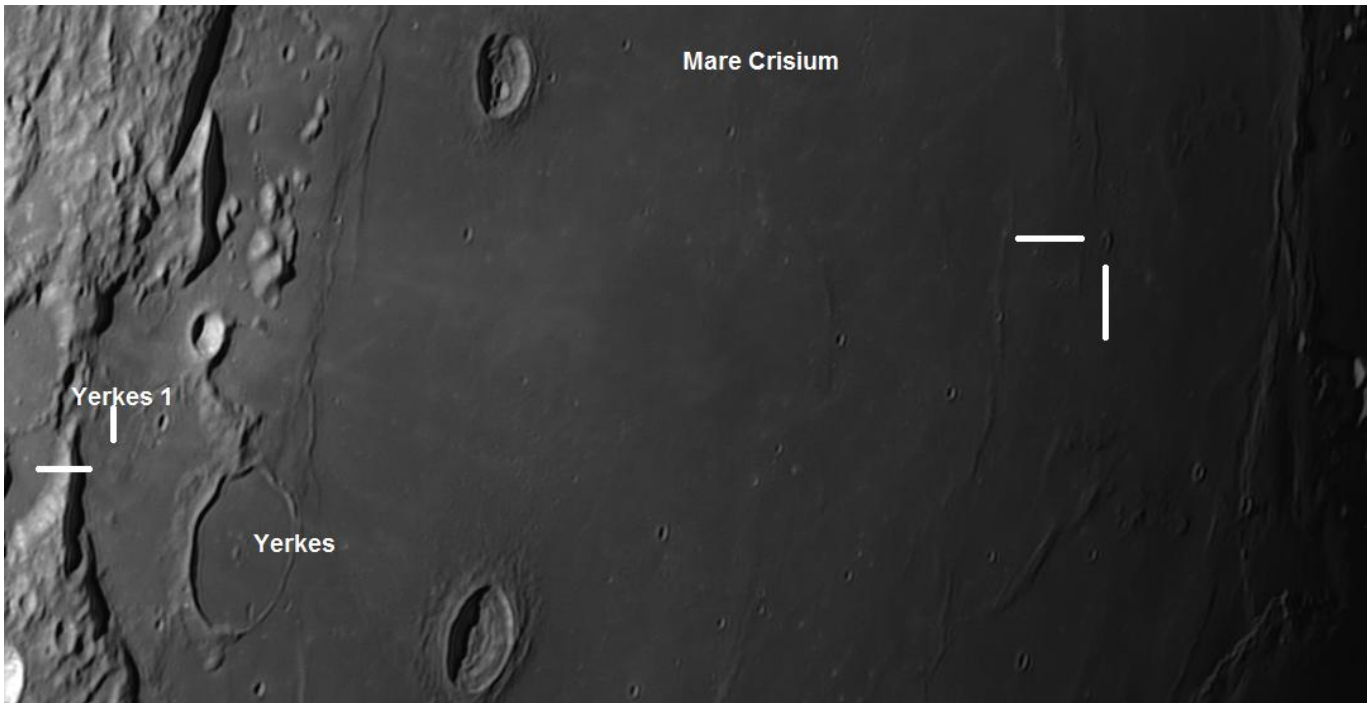

Figure 1: Image taken by Teodorescu using a 355 mm Newtonian telescope and ASI 174MM camera. The examined feature is marked with white lines. Note to the east the dome Yerkes 1.

An enlarged image of this horseshoe like-cone is shown in Fig. 2. This could be of the same nature as the so-called cinder cone near Lassell D (Lena et al., 2013).

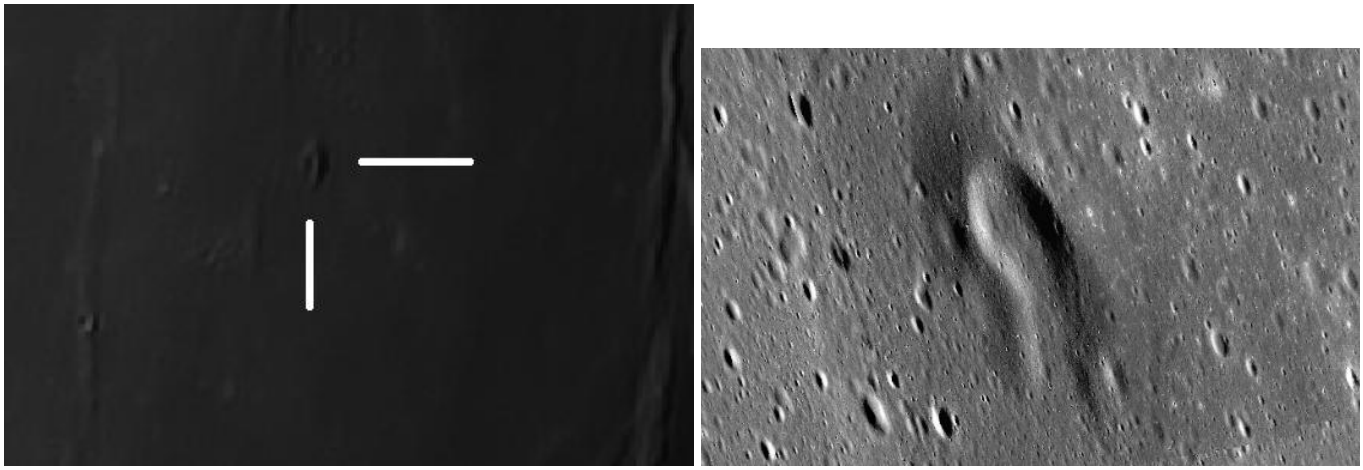

Figure 2: (left) Enlarged image of the feature taken by Teodorescu using a 355 mm Newtonian telescope and ASI 174MM camera. The examined feature is marked with white lines. (Right) WAC image of the feature described in this work.

Another image of this region was made by Robert Cazilhac on December 21, 2021 using a Schmidt Cassegrain 12"F/D20 and an ASI 1600 MMC camera (Fig. 3).

Figure 3: *Image taken by Cazilhac. The examined feature is marked with white lines. In this image north is to the bottom on the left.*

In the USGS I-707, Cleomedes quadrangle, it is described as *Eid unit* corresponding to small irregular dome with relatively large and breached depression at summit, likely a lunar cone:
https://www.lpi.usra.edu/resources/mapcatalog/usgs/I707/150dpi.jpg
As visible in Fig. 4, the WAC image of this feature shows its real nature. In Fig. 4 the foreshortening effect is deleted and the image is seen as cylindrical projection.
It has a breached rim and displays a lava channel starting from the summit, which is also detectable in terrestrial images (see Figs. 1-3).
Lunar volcanic cones form from explosive eruptions with the release of large amounts of dissolved gas (called degassing) when viscous magma rises to slowly fill the volcanic vent.

ACT-REACT Quick Map tool was used to access to the LOLA DEM dataset, obtaining the cross-sectional profile (Figs. 5-6). The examined cone is topographically higher by about 180± 20m than its surroundings. The diameter is determined to 6.0 ± 0.3km, yielding an average flank slope angle of 3.4° ± 0.3° but in some part the slope angle amounts to 8°.

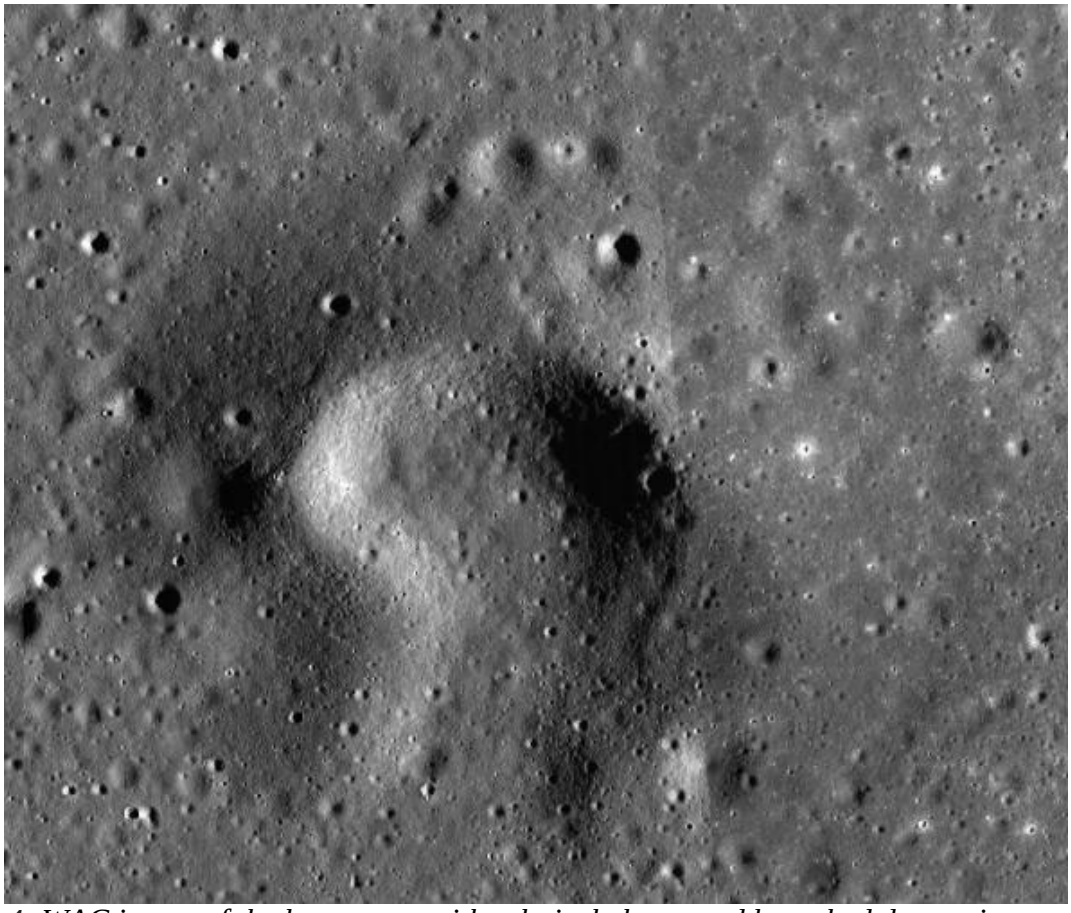

Figure 4: WAC image of the lunar cone with relatively large and breached depression at summit.

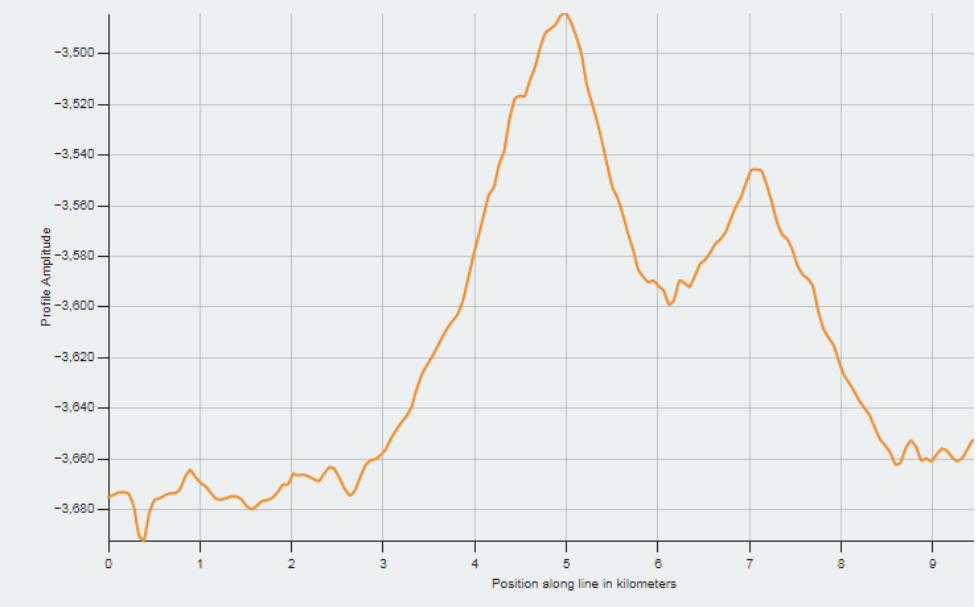

Figure 5: LRO WAC-derived surface elevation plot in East-West direction based on LOLA DEM.

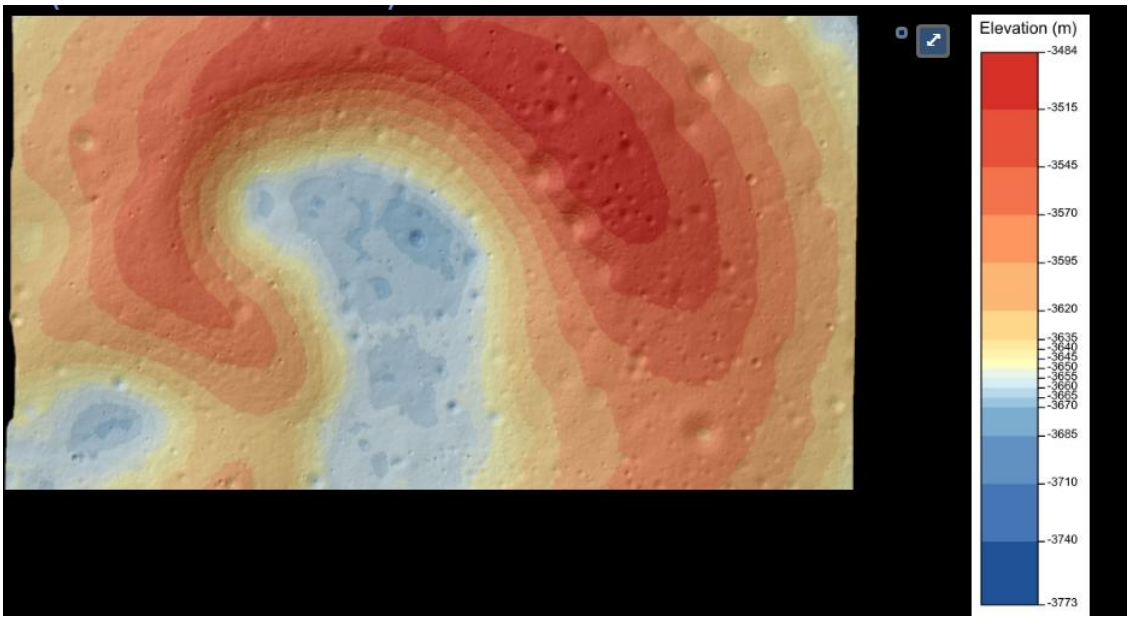

Figure 6: ACT REACT Quick Map tool. Elevation map.

A realistic view based on NAC digital elevation-*QuickMap Terrain Shadows*- displays the shape of the volcanic construct (3D reconstruction shown in Fig. 7).

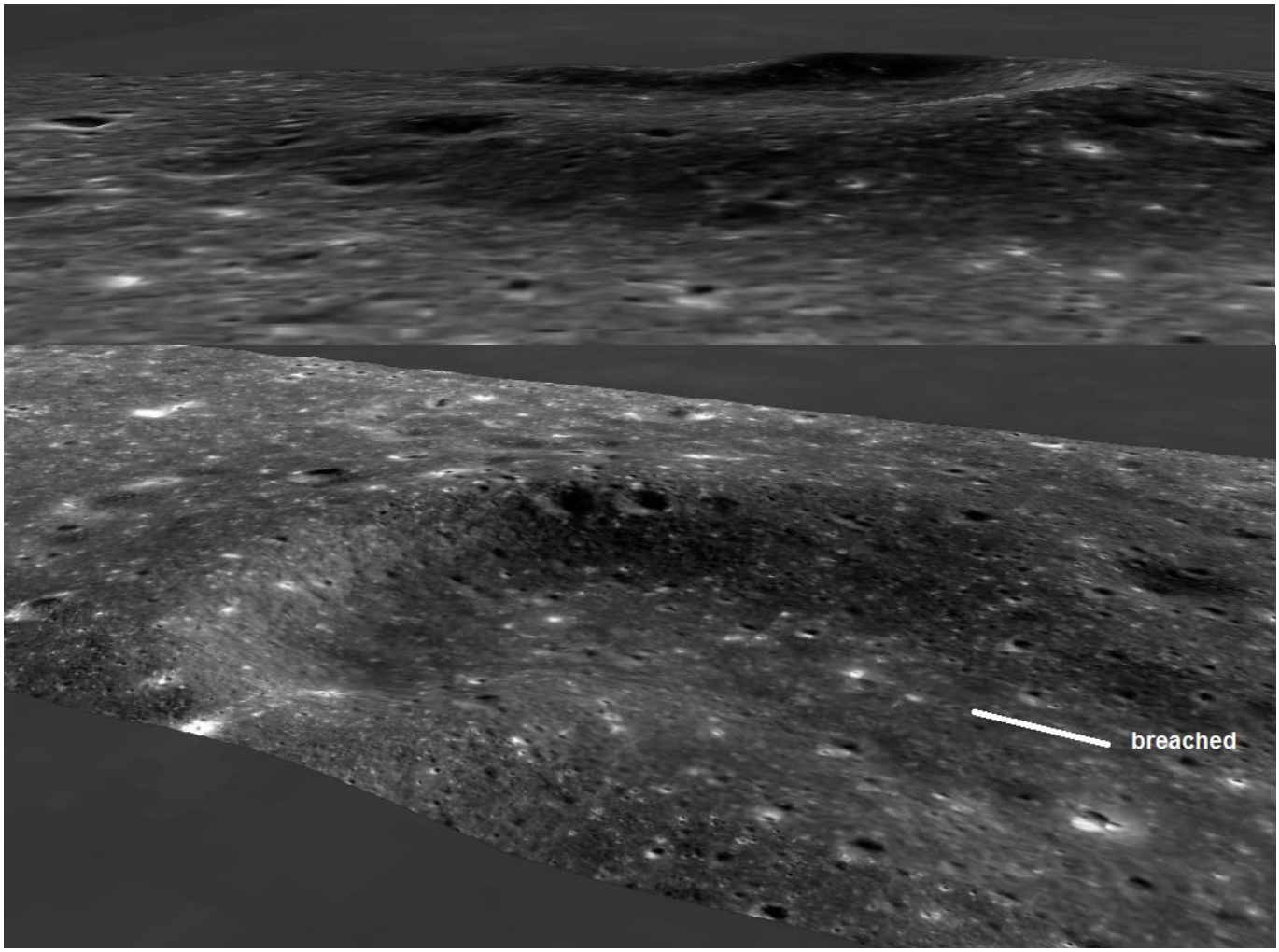

Figure 7: ACT REACT Quick Map tool 3D reconstruction as seen from two different directions based on NAC imagery. Note the breached rim and the lava channel.

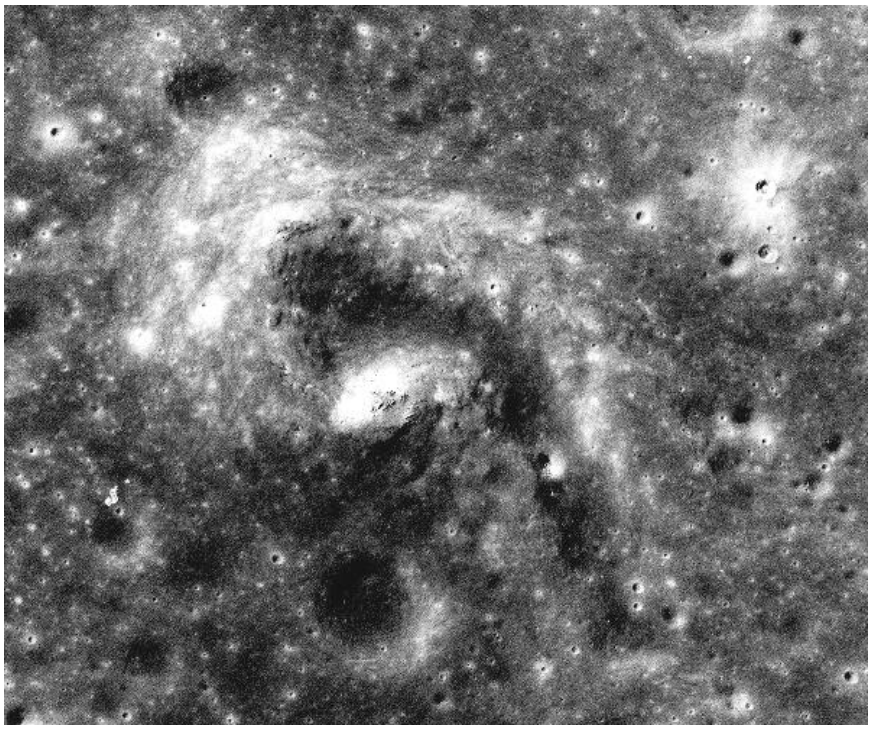

Figure 8: Apollo imagery showing the breached cone Isis in Mare Serenitatis. AS17-P-2760.

The features under investigation can be compared with the known cones Isis and Osiris. Isis, located in Mare Serenitatis (18.96°N, 27.48°E), is a 1.7km diameter cone that is also C-shaped, smooth-sided, and has a gap and a lava channel (Fig. 8). Isis is 60 m in height and has a slope of 4.0°. This feature is similar in morphology to some Marius Hills cones. Osiris is another similar volcanic construct ~2.3 km in diameter, located southeast of Isis (18.60°N, 27.60°E). It does not have a gap in the cone wall. This feature is 70m high, and has a slope of 3.54°. Both of these cones are thus similar to some cones of the Marius Hills, but have lower slopes.
The lunar cone in Crisium, examined in this note, is located in the Im2 unit of Imbrian-age basalts, based on the data described by Lu et al. (2021) corresponding to age of ~3.49 Ga.

Scenarios explaining the observed asymmetry of C-shaped cones include: (1) the non-uniform eruption and emplacement of pyroclastics and lava around the vent resulting in asymmetrical construction of the rim; (2) pre-existing topography directs erupting lavas away from the vent in the downslope direction and prevents the construction of the downslope wall, resulting in an asymmetrical cone; (3) a directional weakness formed in a symmetrical cone due to a pileup of lava and/or pyroclastics on one side results in the collapse of one wall of the cone and is accompanied by a breakout of lava from the cone wall; (4) pre-existing topography controls the flow direction of erupting lavas and results in the destruction of the downslope rim through thermal erosion.

Analyses of the Diviner CF map reveals that it does not display the short wavelength CF position characterizes silica-rich lithologies like the Gruithuisen domes. The average CF position is 8.35 ± 0.05 μm; this value is not different from the average CF position of the typical basaltic *maria*, which is 8.30-8.40μm. Hence, it is not enriched in silica relative to the surrounding mare units.

The mafic minerals (e.g., pyroxene and olivine) of mare basalts can be identified through their characteristic spectral absorption features. Pyroxene displays two absorption peaks at approximately 1,000nm (Band I) and 2,000nm (Band II) (Besse et al., 2014; Klima et al., 2007). In contrast, the olivine reflectance spectrum is revealed by broad and asymmetric 1,000nm absorption, but lacks the 2,000nm absorption. The broad Band I absorption in olivine is caused by three distinct absorption bands [Besse et al., 2011; Besse et al., 2014]. The central absorption, located just beyond 1,000nm, is caused by iron in the M2 crystallographic site. The two weaker absorptions near 850 and 1,250nm are the result of iron in

the M1 site. The Band I "secondary" absorption near 1,250nm allows olivine to be detected when admixed with the spectrally "stronger" pyroxene. The band centers are influenced by the amount of Fe^{2+} and Ca^{2+}: with increasing Fe^{2+} and Ca^{2+}, the band centers move slightly to the longer wavelength. However, in the case of olivine-pyroxene mixtures, Band I is dependent on the relative abundances of both olivine and pyroxene. The spectrum of the cone, derived using M^3 data set, is shown in Fig. 9.

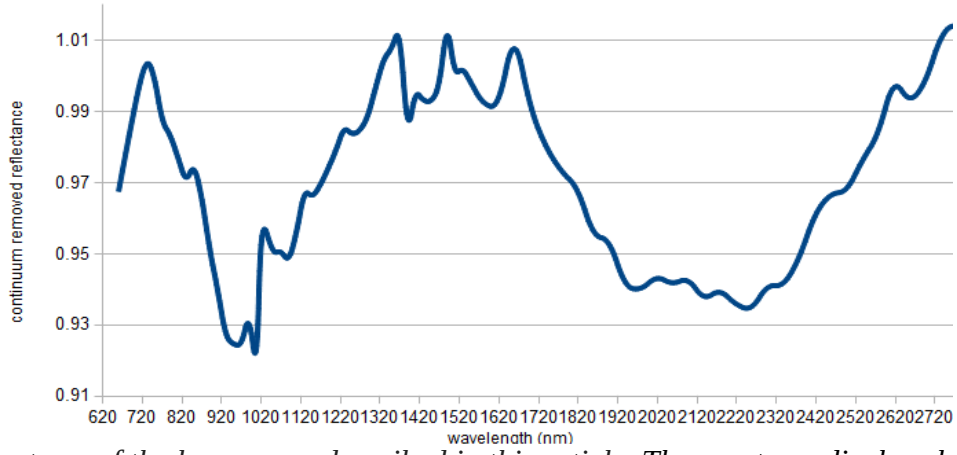

Figure 9: M^3 spectrum of the lunar cone described in this article. The spectrum displays broad, composite absorption feature over 1000nm having the greatest affinity to typical olivine spectra admixed with pyroxenes OP2C1.

Thus the cone displays a mixture of pyroxenes (orthopyrexenes and clinopyroxenes) and olivine. The Multiband Imager (MI) data has been used for compositional analysis. MI is a high-resolution multispectral imaging instrument on board SELENE. It has five visible (VIS) bands (415 nm, 750 nm, 900 nm, 950 nm, and 1000 nm) and four near-infrared bands (1000 nm, 1050 nm, 1250 nm and 1550 nm).

The VIS bands of MI have the same center wavelengths as those of the Clementine UV/VIS camera but have much higher spatial resolution (20 m/pixel). The Clementine color ratio image displays a red color in the area of this breached cone (Fig. 10).

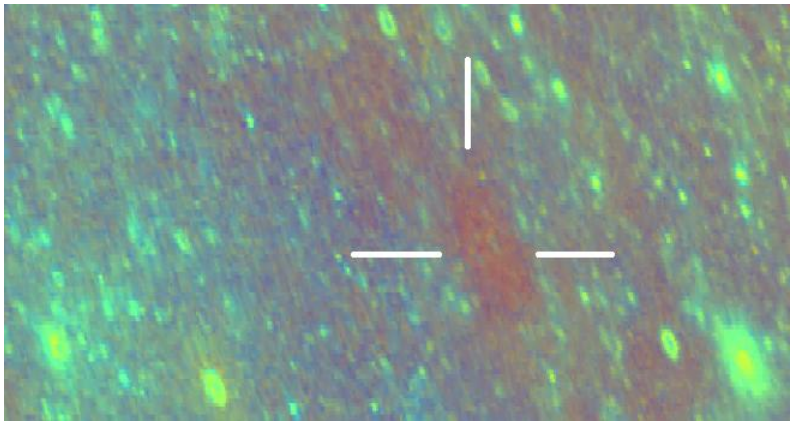

Figure 10: Clementine color ratio image obtained assigning the R_{750}/R_{415}, R_{750}/R_{950} and R_{415}/R_{750} into the red, green, and blue channels, respectively.

Based on the Multiband Imager (MI) dataset the olivine signatures are also detected on the rims and floor of small craters (Figure 11) and inside and outside of the described lunar cone. In these small craters, small-body impact events were able to excavate and expose substrate olivine-rich materials in the lunar subsurface. The highest olivine concentrations identified in the lunar cone may represent a final product slightly differing in olivine rich basaltic composition.

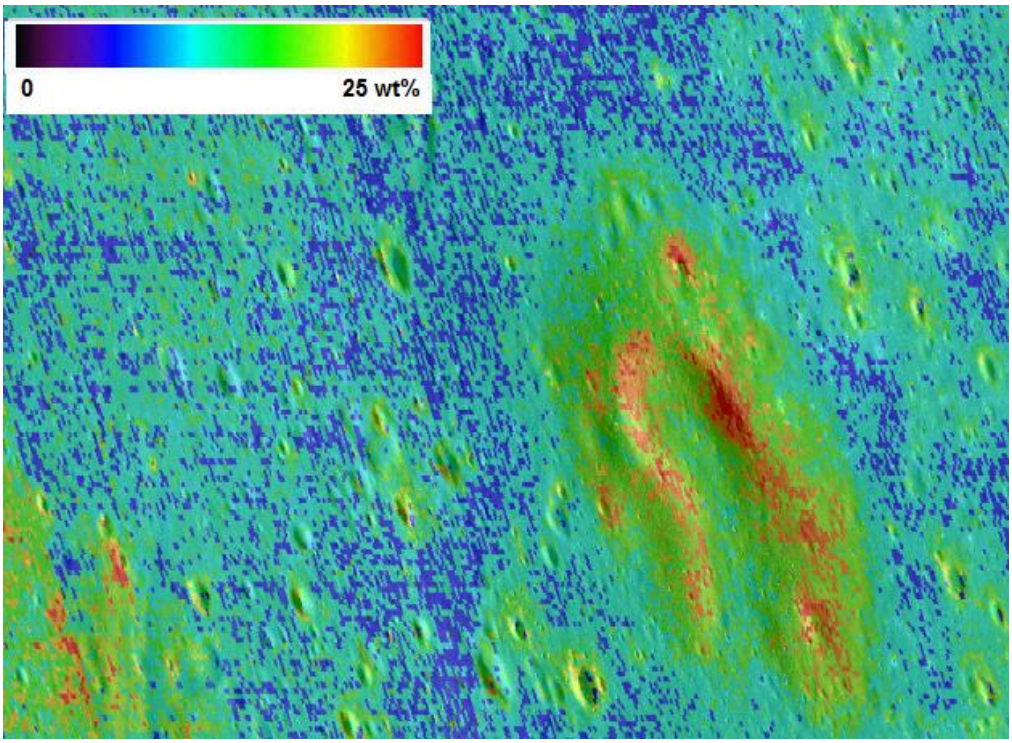

Figure 11: Olivine wt% map of the examined region including the lunar cone.

For this study I have derived abundance maps in wt% of FeO, plagioclase, olivine, clinopyroxene, orthopyroxene and TiO_2 content created from topographically-corrected Mineral Mapper reflectance data acquired by the JAXA SELENE/Kaguya (Fig. 12).

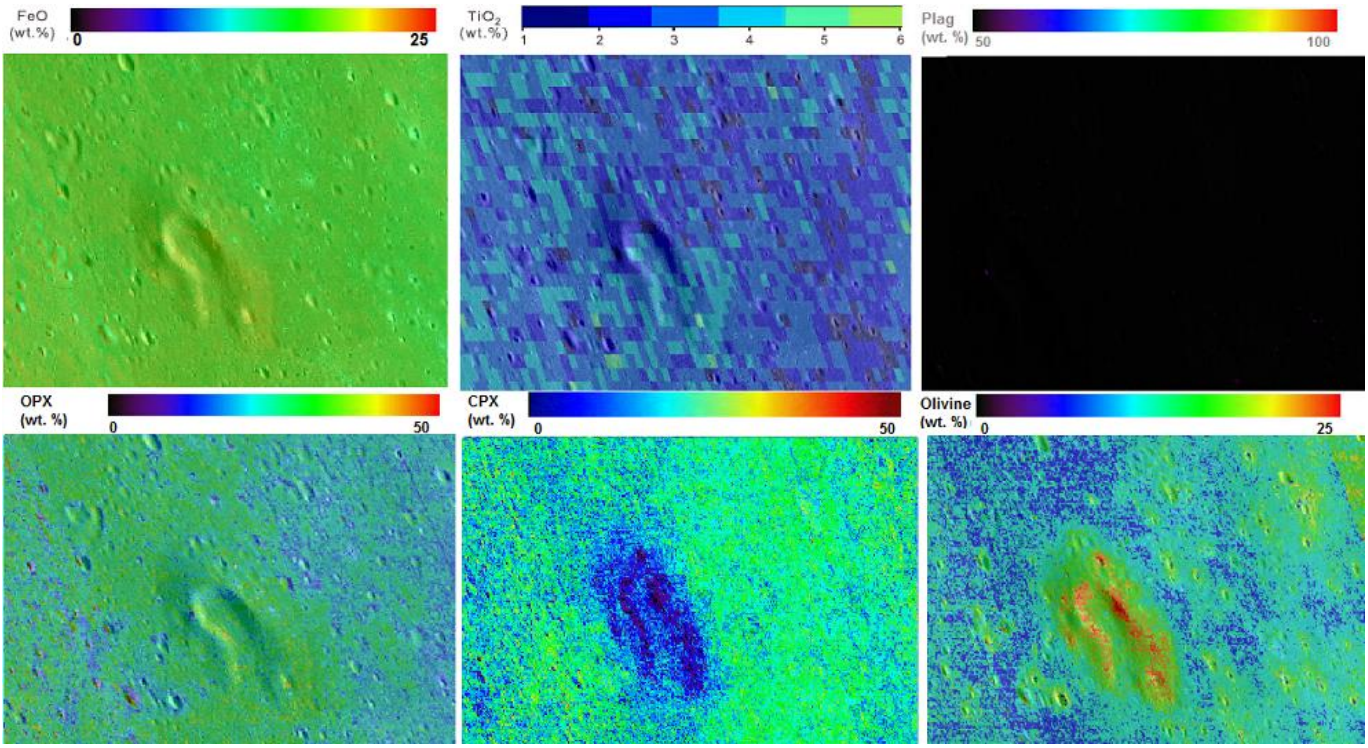

Figure 12: Top (left) Fe0, (middle) $Ti0_2$, (right) plagioclase. Bottom (left) orthopyroxene, (middle) clinopyroxene, (right) olivine content. Derived abundance maps in wt%.

The lunar cone displays a TiO_2 content of 2.0-4.5 wt% and low plagioclase content (<50.0 wt %). The FeO content varies from 16.0 wt % to 19.0 wt % like the nearby mare units.
This lunar cone has an enhanced abundance of orthopyroxene (from 23 wt % to 33 wt %) and a lower abundance of clinopyroxene (5.0-16.0 wt %) if compared with nearby mare units (30-33 wt %). Furthermore the lower clinopyroxene content of the lunar cone is detected where the olivine abundance is higher, suggesting the presence, in the examined region, of different volcanic products of differing composition (Fig. 11).

References

Besse, S., Sunshine, J. M, and Gaddis, L. R. (2014), Volcanic Glass Signatures in Spectroscopic Survey of Newly Proposed Lunar Pyroclastic Deposits, Journal of Geophysical Research - Planets, Vol. 119, doi:10.1002/2013JE004537.

Besse, S., Sunshine, J. M., Staid, M. I., Petro, N. E., Boardman, J. W., Green, R. O., Head, J. W., Isaacson, P. J., Mustard, J. F. and Pieters, C. M. (2011). Compositional variability of the Marius Hills volcanic complex from the Moon Mineralogy Mapper (M^3), J. Geophys. Res., 116, E00G13, doi:10.1029/2010JE003725.

Klima, R. L., C. M. Pieters, and M. D. Dyar (2007), Spectroscopy of synthetic Mg-Fe pyroxenes I: Spin-allowed and spin-forbidden crystal field bands in the visible and near-infrared, Meteorit. Planet. Sci., 42, 235–253.

De Hon, R. A., Mare Spumans and Mare Undarum - Mare thickness and basin floor. Lunar Science Conference, 6th, Houston, Tex., March 17-21, 1975, Proceedings. Volume 3.

Lena, R., Wöhler, C., Phillips, J., Chiocchetta, M.T., 2013. Lunar domes: Properties and Formation Processes, Springer Praxis Books.

Lu, X.; Cao, H.; Ling, Z.; Fu, X.; Qiao, L.; Chen, J. Geomorphology, Mineralogy, and Geochronology of Mare Basalts and Non-Mare Materials around the Lunar Crisium Basin. Remote Sens. 2021, 13, 4828. https:// doi.org/10.3390/rs13234828

Olson, A.; Wilhelms, D.J. *USGS Open-File Report*; U.S. Geological Survey: Flagstaff, AZ, USA, 1974.

Wilhelms, D., The Geologic History of the Moon, USGS Prof. Paper 1348. Washington: GPO, 1987.